Hydrogen Evolution

Deutsche Ausgabe: DOI: 10.1002/ange.201507529
Internationale Ausgabe: DOI: 10.1002/anie.201507529

Dimeric $[Mo_2S_{12}]^{2-}$ Cluster: A Molecular Analogue of MoS_2 Edges for Superior Hydrogen-Evolution Electrocatalysis

Zhongjie Huang, Wenjia Luo, Lu Ma, Mingzhe Yu, Xiaodi Ren, Mingfu He, Shane Polen, Kevin Click, Benjamin Garrett, Jun Lu, Khalil Amine, Christopher Hadad, Weilin Chen, Aravind Asthagiri,* and Yiying Wu**

Abstract: *Proton reduction is one of the most fundamental and important reactions in nature. MoS_2 edges have been identified as the active sites for hydrogen evolution reaction (HER) electrocatalysis. Designing molecular mimics of MoS_2 edge sites is an attractive strategy to understand the underlying catalytic mechanism of different edge sites and improve their activities. Herein we report a dimeric molecular analogue $[Mo_2S_{12}]^{2-}$, as the smallest unit possessing both the terminal and bridging disulfide ligands. Our electrochemical tests show that $[Mo_2S_{12}]^{2-}$ is a superior heterogeneous HER catalyst under acidic conditions. Computations suggest that the bridging disulfide ligand of $[Mo_2S_{12}]^{2-}$ exhibits a hydrogen adsorption free energy near zero (−0.05 eV). This work helps shed light on the rational design of HER catalysts and biomimetics of hydrogen-evolving enzymes.*

Hydrogen has the highest energy density by weight among all chemical fuels. In recent decades, this has sparked intense research interest in generating hydrogen from water splitting. According to the Sabatier principle, the crucial requirement for an optimal hydrogen evolution reaction (HER) catalyst is a moderate binding of H on the catalytic site, which is reflected by near-zero Gibbs free energy for atomic hydrogen adsorption ($\Delta G_{ads}(H) \approx 0$).[1] A state-of-the-art HER catalyst, such as Pt(111), has a $\Delta G_{ads}(H)$ of only −0.09 eV.[2] Promising advances in finding alternative HER catalysts to noble metals have been made in recent years. One landmark example is molybdenum disulfide (MoS_2). The seminal computational and experimental studies have shown that the edge sites of the MoS_2 planes have excellent catalytic activity for HER ($\Delta G_{ads}(H) = 0.08$ eV), while the (0001) basal planes are inert.[1b,2]

A promising approach is to directly design Mo–S based molecules and clusters that vividly mimic the MoS_2 edge sites. Besides maximizing the edge density, these molecular mimics provide an attractive strategy to freely create, precisely probe, and systematically investigate the various types of active sites. The center of Figure 1 shows a single MoS_2 layer with sulfur-rich edges. Different molecular mimics can potentially be designed, depending on which way the MoS_2 sheet is "cropped". For example, a discrete analogue was reported by integrating the single "Mo–S_2" triangular functional unit into a molecular catalyst for homogeneous HER.[3] Polymeric analogues are also possible when polynuclear Mo–S based clusters are introduced. The cluster $[Mo_3S_{13}]^{2-}$ has been reported to be an advanced heterogeneous HER catalyst very recently,[4] which we view as a trimer analogue. However, compared with the numerous efforts in developing nanostructured MoS_2,[5] there have been few catalytic studies of MoS_2 molecular analogues.

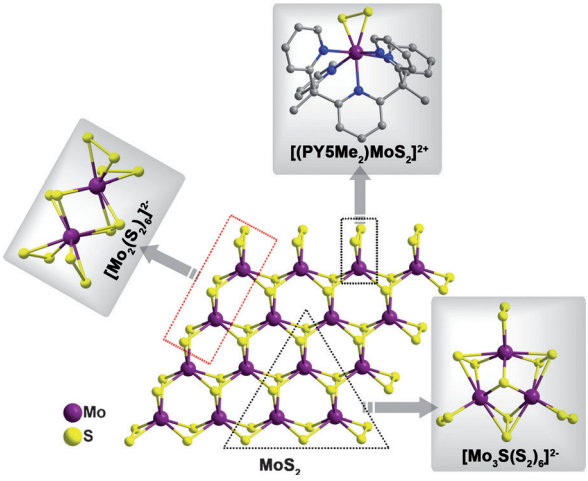

Figure 1. The relationship of the Mo–S based molecular HER catalysts to the monolayer MoS_2 with sulfur-rich edges (center): the discrete analogue $[(PY5Me_2)MoS_2]^{2+}$ (top), the trimeric analogue $[Mo_3S_{13}]^{2-}$ cluster (right), and our dimeric analogue $[Mo_2S_{12}]^{2-}$ cluster (left).

Since the dimer is the smallest unit to possess both terminal and bridging disulfide (S_2) ligands, herein we

[*] Z. Huang, L. Ma, M. Yu, X. Ren, M. He, S. Polen, K. Click, B. Garrett, Prof. C. Hadad, Prof. Y. Wu
Department of Chemistry & Biochemistry, The Ohio State University
100 West 18th Avenue, Columbus, Ohio 43210 (USA)
E-mail: wu@chemistry.ohio-state.edu
W. Luo, Prof. A. Asthagiri
William G. Lowrie Department of Chemical and Biomolecular Engineering, The Ohio State University
140 West 19th Avenue, Columbus, Ohio 43210 (USA)
E-mail: asthagiri.1@osu.edu
Prof. W. Chen
Key Laboratory of Polyoxometalate Science of Ministry of Education
Department of Chemistry, Northeast Normal University
Changchun, Jilin 130024 (China)
E-mail: chenwl@nenu.edu.cn
Prof. J. Lu, Prof. K. Amine
Chemical Sciences and Engineering Division, Argonne National Laboratory
9700 South Cass Avenue, Lemont, Illinois 60439 (USA)

Supporting information and ORCID(s) from the author(s) for this article are available on the WWW under http://dx.doi.org/10.1002/anie.201507529.

conceptually designed a binuclear cluster $[Mo_2S_{12}]^{2-}$ in the form of $(NH_4)_2[Mo_2(S_2)_6]\cdot 2H_2O$, by revisiting classical cluster chemistry. The electrochemical tests show that $[Mo_2S_{12}]^{2-}$ is an advanced heterogeneous HER catalyst under acidic conditions. The comparison of the overpotential and turnover frequency proves the superiority of our $[Mo_2S_{12}]^{2-}$ among the Mo–S based catalysts. The simulated thermoneutral H binding affinity ($(\Delta G_{ads}(H) = -0.05$ eV) is consistent with the high HER catalytic activity.

$(NH_4)_2[Mo_2(S_2)_6]\cdot 2H_2O$ was synthesized and purified based on a modified Müller method.[6] $(NH_4)_2[Mo_2(S_2)_6]\cdot 2H_2O$ was prepared and separated as crystalline black needles/rods with length varying from 10–100 μm (Figure 2b and Figure S2 in Supporting Information). Synchrotron-radiated single-crystal X-ray diffraction (XRD) analysis shows that $(NH_4)_2[Mo_2(S_2)_6]\cdot 2H_2O$ crystallizes in the orthorhombic space group *Pnna* with $a = 21.2927(11)$ Å, $b = 13.0408(7)$ Å, $c = 12.6064(7)$ Å, and a multiplicity of 8 (unit cell depicted in Figure 2c). Figure 2a shows that each Mo center is coordinated to four S_2 units, with two bridging S_2 having a short average S–S bond length of 2.034(5) Å, and two terminal S_2 having a long average S–S bond length of 2.053(2) Å. The details of the single-crystal data, bond angle, and bond length are listed in Table S1–S3. The powder XRD of the bulk sample (Figure S4) is also consistent with the $(NH_4)_2[Mo_2(S_2)_6]\cdot 2H_2O$ phase, proving that our synthesis produces a single-phase product.

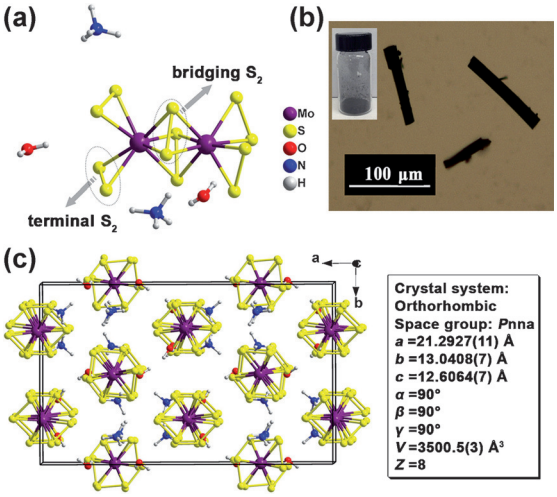

Figure 2. Structure of $(NH_4)_2[Mo_2(S_2)_6]\cdot 2H_2O$. a) Structure of a single molecule, position determined by synchrotron-radiated single-crystal XRD. b) Optical microscopic image of the black rods on a glass slide. Inset: digital image of the bulk powder in the vial. c) The corresponding $(NH_4)_2[Mo_2(S_2)_6]\cdot 2H_2O$ crystal structure, viewed along the *c* axis.

The clusters were drop-casted on an electrode surface. Figure S5 displays the X-ray photoelectron spectroscopy (XPS) spectra of Mo 3d and S 2p region for the as-synthesized crystalline powder sample and the deposited film on fluorine-doped tin oxide (FTO) substrate by drop-casting fresh 1 mM $[Mo_2S_{12}]^{2-}$ dimethylformamide (DMF) solution (Figure S8a). The detailed analysis can be found in the Supporting Information. The spectra for the crystalline powder sample and the deposited film are almost identical, which suggests that the structure of the anionic cluster on the electrode surface is unchanged.

The HER electrocatalytic activities were investigated in 0.5 M H_2SO_4 solution (Ar saturated) with a typical three-electrode setup. The scan rate of all linear sweep voltammetry (LSV) tests was 5 mV s^{-1}. Submonolayer of catalyst was loaded by the layer-by-layer self-assembly method on FTO substrates with the help of a commonly used polycation poly(diallyldimethylammonium chloride).[7] The amount for sub-monolayer loading is 0.17 nmol cm^{-2}, as determined by inductively coupled plasma measurement. The FTO does not shown any detectable transmittance change after one cycle of catalyst loading, however the polarization curve (inset of Figure 3a) clearly demonstrates the activity of the submonolayer of catalyst. Higher amount of catalyst was loaded on the glassy carbon (GC) electrode by drop-casting a homogeneous ink consisting of fresh $[Mo_2S_{12}]^{2-}$ (termed "Mo2") DMF solution, carbon powder, and Nafion. The polarization curves of Mo2 with various catalyst loading amount are displayed in Figure 3a. The bare carbon powder on the GC electrode was relatively inert to HER, with a negligible background current and an overpotential over 600 mV. When Mo2 was present, the polarization curve showed a low overpotential of 100 ~ 150 mV, beyond which the current density rises very rapidly. The cathodic current density enhances with the increasing amount of catalyst loading at a given potential. The HER electrocatalytic activity of Mo2 was compared with that of the commercial bulk MoS_2 powder and the state-of-the-art catalyst $[Mo_3S_{13}]^{2-}$ (termed "Mo3", Figure S6) in Figure 3b. Our performance of Mo3 resembles the earlier reported value (10 nmol cm^{-2} is ca. 7.6 μg cm^{-2}).[4] Furthermore, Figure 3b clearly illustrates that the catalytic activity of Mo2 is superior to that of Mo3 with equivalent mole of catalyst loading. The bulk MoS_2 shows negligible H_2-evolving activity.

Tafel plots can help to elucidate the electron-transfer kinetics. Three possible elementary steps have been suggested for HER in acidic solutions.[8] The first step is an initial discharge step (Volmer reaction) [Eq. (1)]:

$$H_3O^+ + e^- \rightarrow H_{ads} + H_2O \quad (1)$$

followed by either an electrochemical desorption step (Heyrovsky reaction) [Eq. (2)]

$$H_{ads} + H_3O^+ + e^- \rightarrow H_2 + H_2O \quad (2)$$

or a recombination step (Tafel reaction) [Eq. (3)]

$$H_{ads} + H_{ads} \rightarrow H_2 \quad (3)$$

The HER reaction involves steps of either Equations (1)–(2) or (1)–(3). Assuming the symmetric coefficient is 0.5, the Tafel slope should be around 120, 40, or 30 mV dec^{-1}, if the rate limiting step is Equation (1), (2), or (3), respectively.

The Tafel slope is 40 and 39 mV dec^{-1} for our Mo3 and Mo2 sample, respectively (Figure 3c). The result of Mo3 agrees with the literature.[4] Beyond the linear region, the current density deviates from the exponential relationship at

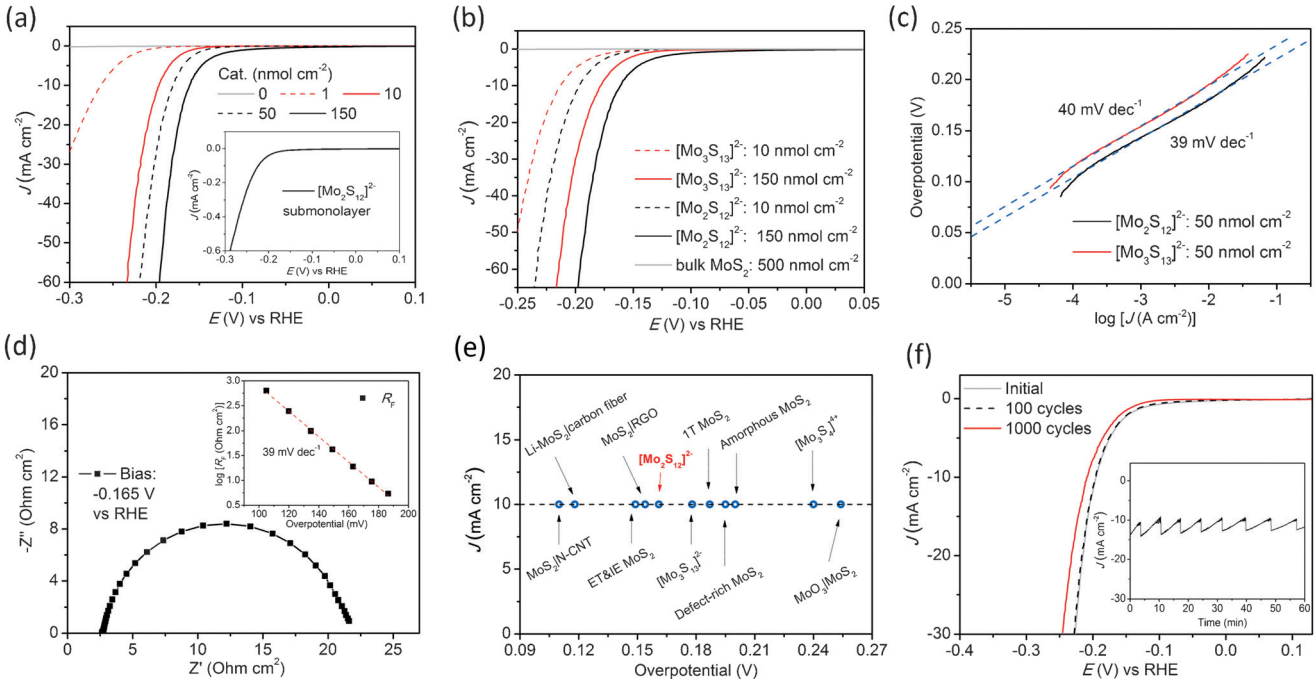

Figure 3. Electrochemistry tests of the HER catalytic activity. a) Polarization curves with different $[Mo_2S_{12}]^{2-}$ catalyst loading. Inset: the performance of sub-monolayer deposited cluster on FTO electrode. b) Polarization curves with $[Mo_2S_{12}]^{2-}$, $[Mo_3S_{13}]^{2-}$, and bulk MoS_2. c) Tafel plots of the polarization curves. d) Nyquist plots at the bias of −0.165 V. Inset: the exponential dependence of R_F with overpotential. e) Comparison of the overpotential at 10 mA cm^{-2} for various Mo–S based catalysts. f) Polarization curves recorded before and after 100 and 1000 cycles of accelerated stability scan. Inset: the *J*–*t* response in a chronoamperometry test. Except for the inset of Figure 1, all the other data were obtained on GC electrode.

higher overpotentials, which might be due to the diffusion limit or blocking of the catalytic site by generated hydrogen bubbles.[4] The Tafel slope of approximately 40 mV dec^{-1} indicates that both clusters proceed via the Volmer–Heyrovsky (Equation (1)–(2)) mechanism, and the electrochemical desorption step (Heyrovsky reaction) is the rate limiting step. Tafel slopes of the reported advanced alternative HER catalysts are summarized in Table S4. Mo2 is among the types of clusters with a small Tafel slope, which means that significant enhancement of the catalytic current can be obtained with only a moderate increase of the overpotential. The only alternative HER catalyst with an apparently smaller Tafel slope is the polypyrrole and MoS_x copolymer film (29 mV dec^{-1}).[9]

Electrochemical impedance spectroscopy (EIS) was used to probe the electrochemical and ionic process at the electrode/electrolyte interface. We performed EIS under different dc bias along the *j*–*V* curve. Representative Nyquist plots (bias: −0.165 V) are presented in Figure 3d, and the width of the semicircle indicates the total Faradic resistance of the HER process.[5a,i,10] The Faradic resistances of Mo2 (10 nmol cm^{-2}) under different overpotentials (after *iR* correction) are displayed in the inset of Figure 3d. The Faradic resistance drops exponentially as the overpotential increases, and the slope is in excellent agreement with the Tafel slope.

For comparing the HER activity of different heterogeneous catalysts, Jaramillo et al. suggested the overpotential at 10 mA cm^{-2} electrode as a crucial parameter for evaluation.[5h] As displayed in Figure 3e, Mo2 only requires an overpotential of 161 mV to reach a *J* of 10 mA cm^{-2}, outperforming other cluster-type catalysts, such as $[Mo_3S_4]^{4+}$ (240 mV)[11] and Mo3 (178 mV in this work and 174 mV in Ref. [4]), and most MoS_2 or MoS_3 based materials.[5a,d,i,12] We also compare the turnover frequency (TOF) of these catalysts at a 200 mV overpotential (Table S5). The TOF is normalized to per Mo atom in the catalyst based on the loading mass, because Mo is at least 100 times more expensive than S, and the accurate definition and evaluation of the exact amount of the "active catalytic site" is complicated for different reported results. Mo2 shows a TOF of 3.27 ± 0.15 s^{-1} per Mo (from three independent measurements) with the catalyst loading amount of 6.5 μg cm^{-2}, which is higher than most of the Mo–S based catalysts with similar loading mass. The highest TOF so far is obtained from MoS_2 nanoparticles on the precious metal electrode Au(111),[1b,5f] which is marginally higher than that of Mo2.

Stability is also an important parameter for practical applications. We applied an accelerated cyclic potential scan from 0.2 V to −0.25 V at a scan rate of 100 mV s^{-1}. Only marginal activity loss was observed for Mo2 (10 nmol cm^{-2}) modified glassy carbon (GC) electrode: the overpotential at 10 mA cm^{-2} increased by 1 and 13 mV for the scan after 100 and 1000 potential cycles, respectively (Figure 3f). This stability is similar to that of $[Mo_3S_{13}]^{2-}$, which witnessed an increase by 13 mV in a similar stability test.[5h] A chronoamperometry (CA) test was performed on a rotating disk electrode (RDE) with 20 nmol cm^{-2} of Mo2 at a bias of −0.2 V. Even at a rotating speed of 2500 r.p.m, hydrogen

bubbles kept accumulating in situ (Figure S8b) as a result of the remarkable current, which blocked the electrode surface and lead to the fluctuation of the current (bubble growing/bursting). The overall trend shows a decent retention of the performance. The chemical stability of the catalyst after 1 h CA test on the FTO electrode was carefully investigated by XPS (Figure S10) and Raman spectra (Figure S11). The cyclability, and the similarity of the XPS and Raman spectra of the electrode before and after the stability test demonstrate that Mo2 is a stable HER catalyst in acidic solution.

Nørskov and co-workers illustrated that the binding affinity of H is an excellent descriptor of the HER activity of materials.[1a,13] The origin of the excellent HER activity of our catalyst is studied by density functional theory (DFT) calculations. We systematically explored the adsorption of H on various sites of Mo2. The catalytic paths through Mo–H or S–H intermediates have both been reported for Mo–S based materials.[2,14] Our Mo atom has a high coordination number environment, making the Mo–H binding not preferable. The preferred initial hydrogen binding position is suggested to be a bridging S_2 (Figure 4a) with $\Delta G_{ads}(H)$ of −0.05 eV (compared to 0.02 eV for terminal S_2, see Figure S12a). Since multiple H adsorption sites exist, we also examined the possibility of the second (and further) H adsorption on Mo2. We found that the adsorption of the second H will increase the free energy of the system by at least 0.19 eV (Figure S12b), which is much higher than the potential necessary to desorb the first H atom through reaction: $H{-}Mo2 + H^+ + e^- \rightarrow Mo2 + H_2$ ($\Delta G = 0.05$ eV). Since the second (and further) H adsorption is endothermic, we would expect only one H adsorbed in the catalytic cycle at approximately 0 V versus RHE. The preference of 1 H adsorption over 2 H adsorption is revealed in the catalytic pathway shown in Figure 4a. This observation also suggests that the Tafel step is not favored compared with Heyrovsky reaction because the Tafel step requires at least two adsorbed H. Even at more negative bias, the Tafel step needs a large activation energy barrier of 0.91 eV, therefore the Volmer–Heyrovsky mechanism should dominate, which is consistent with the experimental Tafel plot (Figure 3c).

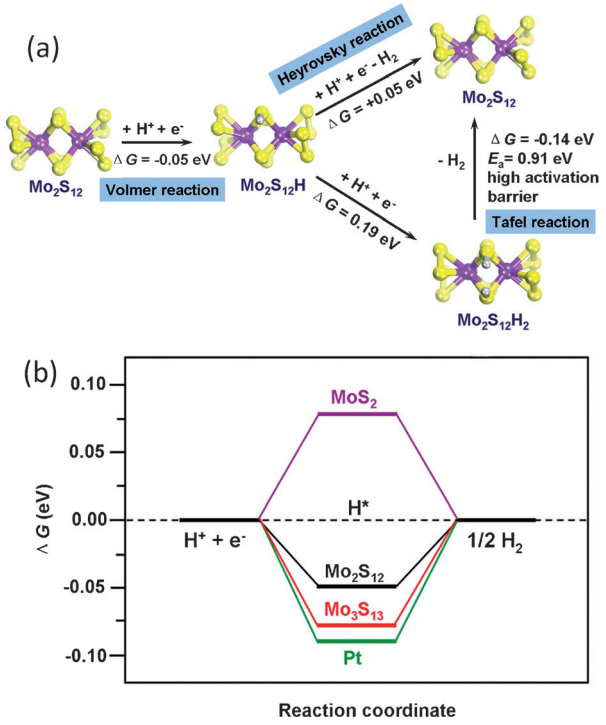

Figure 4. a) Catalytic reaction pathways and energies of the HER on Mo2 with two different reaction mechanisms (Volmer–Heyrovsky or Volmer–Tafel reaction). b) Energetics of HER process on different catalysts: Mo2, Mo3, MoS_2 nanoparticle and Pt.

The free-energy changes during HER based on the Volmer–Heyrovsky reaction are shown in the energy diagram in Figure 4b. Mo2 shows a close-to-zero $\Delta G_{ads}(H)$ of −0.05 eV, in comparison to Mo3 (calculated by us as −0.08 eV), MoS_2 nanoparticles (0.08 eV),[2] and Pt(111) (−0.09 eV).[1a] Mo2 shows a smaller $|\Delta G_{ads}(H)|$ than Mo3, which agrees well with the trend of the catalytic activity. The $|\Delta G_{ads}(H)|$ of Mo2 is smaller than other reported moderate metallic catalysts[1a] and the recently reported advanced catalysts (−0.19 eV for C_3N_4@NG and 0.40 eV for Mo_3S_4).[10b,15]

To summarize, the $[Mo_2S_{12}]^{2-}$ cluster is reported as an advanced heterogeneous HER electrocatalyst and the simplest molecular model for the mimic and investigation of the terminal and bridging S_2. The crystal structure of the $(NH_4)_2[Mo_2(S_2)_6]\cdot 2H_2O$ microrod was well characterized by synchrotron-radiated single-crystal XRD. The catalyst can be loaded on GC and FTO electrodes by the drop-casting method. The small Tafel slope of approximately 40 mV dec^{-1} suggests that the HER process goes through the Volmer–Heyrovsky mechanism, with the Heyrovsky reaction as the rate limiting step. The comparison of the overpotential and turnover frequency indicates the superiority of $(NH_4)_2[Mo_2(S_2)_6]\cdot 2H_2O$ over most of the other Mo–S based catalysts. The hydrogen adsorption energy is calculated to be only −0.05 eV on the bridging S_2, which is the best value among all the reported non-metallic HER catalysts. These results indicate that the $[Mo_2S_{12}]^{2-}$ cluster has promising HER applications in the electrolysis and photoelectrolysis of water. Furthermore, rich chemistry can be applied in the MoS_2 molecular mimics, for the design and precise investigation of different types of active sites. We think our study is helpful shedding light on the rational design of HER catalysts and biomimetics of hydrogen-evolving enzymes.

Acknowledgements

We acknowledge the financial support from the U.S. Department of Energy (DOE) (Award No. DE-FG02-07ER46427). Crystallographic data were collected through the SCrALS program at Beamline 11.3.1 at the Advanced Light Source (ALS), Lawrence Berkeley National Laboratory, which is supported by the U.S. DOE, Office of Energy Sciences Materials Sciences Division, under contract DE-AC02-05CH11231. We thank the Ohio Supercomputer Center for providing computational resources, and Dr. Judith Gallucci

for help in single-crystal characterization. J. L. and K. A acknowledge the support from the U.S. Department of Energy under Contract DE-AC0206CH11357 with the main support provided by the Vehicle Technologies Office, Department of Energy (DOE) Office of Energy Efficiency and Renewable Energy (EERE).

Keywords: electrocatalysis · hydrogen adsorption energy · hydrogen evolution · molecular analogues · molybdenum sulfide

How to cite: *Angew. Chem. Int. Ed.* **2015**, *54*, 15181–15185
Angew. Chem. **2015**, *127*, 15396–15400

[1] a) J. K. Nørskov, T. Bligaard, A. Logadottir, J. R. Kitchin, J. G. Chen, S. Pandelov, U. Stimming, *J. Electrochem. Soc.* **2005**, *152*, J23–J26; b) T. F. Jaramillo, K. P. Jorgensen, J. Bonde, J. H. Nielsen, S. Horch, I. Chorkendorff, *Science* **2007**, *317*, 100–102.

[2] B. Hinnemann, P. G. Moses, J. Bonde, K. P. Jorgensen, J. H. Nielsen, S. Horch, I. Chorkendorff, J. K. Norskov, *J. Am. Chem. Soc.* **2005**, *127*, 5308–5309.

[3] H. I. Karunadasa, E. Montalvo, Y. Sun, M. Majda, J. R. Long, C. J. Chang, *Science* **2012**, *335*, 698–702.

[4] J. Kibsgaard, T. F. Jaramillo, F. Besenbacher, *Nat. Chem.* **2014**, *6*, 248–253.

[5] a) Y. Li, H. Wang, L. Xie, Y. Liang, G. Hong, H. Dai, *J. Am. Chem. Soc.* **2011**, *133*, 7296–7299; b) D. Merki, X. Hu, *Energy Environ. Sci.* **2011**, *4*, 3878–3888; c) J. Kibsgaard, Z. Chen, B. N. Reinecke, T. F. Jaramillo, *Nat. Mater.* **2012**, *11*, 963–969; d) M. A. Lukowski, A. S. Daniel, F. Meng, A. Forticaux, L. Li, S. Jin, *J. Am. Chem. Soc.* **2013**, *135*, 10274–10277; e) H. Wang, Z. Lu, S. Xu, D. Kong, J. Cha, G. Zheng, P. Hsu, K. Yan, D. Bradshaw, F. Prinz, Y. Cui, *Proc. Natl. Acad. Sci. USA* **2013**, *110*, 19701–19706; f) T. Wang, L. Liu, Z. Zhu, P. Papakonstantinou, J. Hu, H. Liu, M. Li, *Energy Environ. Sci.* **2013**, *6*, 625–633; g) J. Xie, J. Zhang, S. Li, F. Grote, X. Zhang, H. Zhang, R. Wang, Y. Lei, B. Pan, Y. Xie, *J. Am. Chem. Soc.* **2013**, *135*, 17881–17888; h) J. D. Benck, T. R. Hellstern, J. Kibsgaard, P. Chakthranont, T. F. Jaramillo, *ACS Catal.* **2014**, *4*, 3957–3971; i) M. Gao, M. Chan, Y. Sun, *Nat. Commun.* **2015**, *6*, 7493; j) M. Gao, J. Liang, Y. Zheng, Y. Xu, J. Jiang, Q. Gao, J. Li, S. Yu, *Nat. Commun.* **2015**, *6*, 5982.

[6] a) A. Müller, W.-O. Nolte, B. Krebs, *Angew. Chem. Int. Ed. Engl.* **1978**, *17*, 279–279; *Angew. Chem.* **1978**, *90*, 286–287; b) A. Müller, S. Sarkar, R. G. Bhattacharyya, S. Pohl, M. Dartmann, *Angew. Chem. Int. Ed. Engl.* **1978**, *17*, 535–535; *Angew. Chem.* **1978**, *90*, 564–565; c) A. Müller, R. G. Bhattacharyya, B. Pfefferkorn, *Chem. Ber.* **1979**, *112*, 778–780; d) A. Müller, E. Krickemeyer, A. Hadjikyriacou, D. Coucouvanis in *Inorg. Synth.*, Wiley, Hoboken, **2007**, pp. 47–51.

[7] H. Fukumoto, Y. Yonezawa, *Thin Solid Films* **1998**, *327*, 748–751.

[8] B. E. Conway, B. V. Tilak, *Electrochim. Acta* **2002**, *47*, 3571–3594.

[9] T. Wang, J. Zhuo, K. Du, B. Chen, Z. Zhu, Y. Shao, M. Li, *Adv. Mater.* **2014**, *26*, 3761–3766.

[10] a) M. S. Faber, R. Dziedzic, M. A. Lukowski, N. S. Kaiser, Q. Ding, S. Jin, *J. Am. Chem. Soc.* **2014**, *136*, 10053–10061; b) Y. Zheng, Y. Jiao, Y. H. Zhu, L. H. Li, Y. Han, Y. Chen, A. J. Du, M. Jaroniec, S. Z. Qiao, *Nat. Commun.* **2014**, *5*, 3783.

[11] T. F. Jaramillo, J. Bonde, J. Zhang, B.-L. Ooi, K. Andersson, J. Ulstrup, I. Chorkendorff, *J. Phys. Chem. C* **2008**, *112*, 17492–17498.

[12] a) Z. Chen, D. Cummins, B. N. Reinecke, E. Clark, M. K. Sunkara, T. F. Jaramillo, *Nano Lett.* **2011**, *11*, 4168–4175; b) J. Xie, H. Zhang, S. Li, R. Wang, X. Sun, M. Zhou, J. Zhou, X. Lou, Y. Xie, *Adv. Mater.* **2013**, *25*, 5807–5813; c) D. Li, U. Maiti, J. Lim, D. Choi, W. Lee, Y. Oh, G. Lee, S. Kim, *Nano. Lett.* **2014**, *14*, 1228–1233; d) H. Wang, Z. Lu, D. Kong, J. Sun, T. Hymel, Y. Cui, *ACS Nano* **2014**, *8*, 4940–4947; e) J. D. Benck, Z. Chen, L. Y. Kuritzky, A. J. Forman, T. F. Jaramillo, *ACS Catal.* **2012**, *2*, 1916–1923.

[13] a) J. Greeley, T. F. Jaramillo, J. Bonde, I. B. Chorkendorff, J. K. Norskov, *Nat. Mater.* **2006**, *5*, 909–913; b) J. K. Nørskov, T. Bligaard, J. Rossmeisl, C. H. Christensen, *Nat. Chem.* **2009**, *1*, 37–46.

[14] a) Y. Huang, R. J. Nielsen, W. A. Goddard, M. P. Soriaga, *J. Am. Chem. Soc.* **2015**, *137*, 6692–6698; b) B. Lassalle-Kaiser, D. Merki, H. Vrubel, S. Gul, V. K. Yachandra, X. Hu, J. Yano, *J. Am. Chem. Soc.* **2015**, *137*, 314–321; c) A. M. Appel, D. L. DuBois, M. R. DuBois, *J. Am. Chem. Soc.* **2005**, *127*, 12717–12726.

[15] Y. Hou, B. L. Abrams, P. C. K. Vesborg, M. E. Bjorketun, K. Herbst, L. Bech, A. M. Setti, C. D. Damsgaard, T. Pedersen, O. Hansen, J. Rossmeisl, S. Dahl, J. K. Norskov, I. Chorkendorff, *Nat. Mater.* **2011**, *10*, 434–438.

Received: August 12, 2015
Published online: October 20, 2015

